Eur. Phys. J. D **13**, 305–316 (2001)

THE EUROPEAN PHYSICAL JOURNAL D

EDP Sciences

Collisional quenching of metastable states of antiprotonic helium by hydrogen and deuterium molecules

B. Ketzer[1,a], T. von Egidy[1], F.J. Hartmann[1], C. Maierl[1], R. Pohl[1,b], J. Eades[2], E. Widmann[2,c], T. Yamazaki[2,d], M. Kumakura[3], N. Morita[3], R.S. Hayano[4], M. Hori[4], T. Ishikawa[4], H.A. Torii[4,e], I. Sugai[5], and D. Horváth[6]

[1] Physik-Department, Technische Universität München, 85747 Garching, Germany
[2] CERN, European Organization for Nuclear Research, 1211 Genève 23, Switzerland
[3] Institute for Molecular Science, Myodaiji, Okazaki 444, Japan
[4] Department of Physics, University of Tokyo, 7-3-1 Hongo, Bunkyo-ku, Tokyo 113, Japan
[5] Institute of Particle and Nuclear Studies, 3-2-1 Midori-cho, Tanashi, Tokyo 188-8501, Japan
[6] Central Research Institute for Physics, Research Institute for Particle and Nuclear Physics, 1525 Budapest, Hungary

Received 2 October 2000

Abstract. The quenching of metastable states of antiprotonic helium by collisions with hydrogen and deuterium molecules was studied. A systematic investigation of the delayed annihilation time spectra at various H_2 and D_2 admixture ratios at the ppm level revealed characteristic changes of their shape, which indicated a strong principal and orbital quantum number dependent quenching of levels in both cases. Applying a laser spectroscopy technique to measure the lifetimes of individual states and cascades we deduced H_2 and D_2 quenching cross-sections for the states $(n, l) = (39, 35)$ and $(37, 34)$. These cross-sections establish for D_2 molecules the strong increase of the quenching efficiency with increasing principal quantum number n of the state under investigation previously reported for the case of H_2 admixtures. Our experiments indicate that the low-n state $(37, 34)$ is somewhat less affected by D_2 than by H_2, while the high-n state $(39, 35)$ is equally quenched by both isotopes.

PACS. 36.10.-k Exotic atoms and molecules (containing mesons, muons, and other unusual particles) – 42.62.Fi Laser spectroscopy – 34.20.Gj Intermolecular and atom-molecule potentials and forces

1 Introduction

An antiproton ($\overline{p}$) stopped in ordinary matter is captured by the Coulomb force into an atomic orbit around the nucleus of a target atom, thereby liberating one of its electrons [1]. This newly formed exotic atom usually disintegrates within a few picoseconds due to the almost instantaneous absorption of the antiproton by the nucleus. A remarkable exception to this rule was discovered in helium, where a small fraction of antiprotons ($\approx 3\%$) was observed to survive as long as several microseconds [2–7]. No evidence for such delayed annihilation was found in liquid nitrogen or liquid argon [2], solid metallic lithium, LiH or LiF [5], and gaseous neon [4,5], krypton or xenon [5]. Apparently, the capture of antiprotons into metastable states is unique to helium.

After its slowing down in inelastic collisions with atomic electrons of helium, the antiproton is initially captured into a state which closely overlaps that of the electron it displaces. In a simple single-particle approximation using hydrogen-like wavefunctions, the orbits of the electron, which is assumed to be in the $1s$ ground state before capture, and of the antiproton, which immediately after capture occupies a state with principal quantum number n, are characterized by the Bohr radii

$$r_{\mathrm{B}}^{e} = \frac{1}{z} a_0,$$
$$r_{\mathrm{B}}^{\overline{p}} = \frac{m_e}{M} \frac{n^2}{Z} a_0,$$

where m_e is the electron mass, M is the $\overline{p}$–He^{2+} reduced mass, Z, z are effective charges to account for the screening of the nuclear charge by the remaining electron of the antiprotonic and purely electronic atom, respectively, and $a_0 = 4\pi\epsilon_0\hbar^2/m_e e^2$ is the Bohr radius. Maximum overlap of antiproton and electron orbits implies that $r_{\mathrm{B}}^{\overline{p}} = r_{\mathrm{B}}^{e}$, which also means $Z = z$. The principal quantum number

[a] *Present address:* CERN, European Organization for Nuclear Research, 1211 Genève, Switzerland.
e-mail: `bernhard.ketzer@cern.ch`
[b] *Present address:* Paul Scherrer Institut, 5232 Villigen PSI, Switzerland.
[c] *Present address:* Department of Physics, University of Tokyo, 7-3-1 Hongo, Bunkyo-ku, Tokyo 113, Japan.
[d] *Present address:* RIKEN, Wako 351-01, Japan.
[e] *Present address:* Institute of Physics, University of Tokyo, 3-8-1 Komaba, Meguro-ku, Tokyo 153-8902, Japan.

of the initially populated state can then be estimated to be $n \approx n_0 \equiv \sqrt{M/m_e} \approx 38$, if the helium atom was in the $1s^2$ ground state before capture. The total energy of the antiprotonic helium atom $\overline{p}\mathrm{He}^+$ ($\equiv \overline{p}e\mathrm{He}^{2+}$) immediately after capture is thus

$$E^{\overline{p}\mathrm{He}^+} \approx -\frac{Mc^2\alpha^2Z^2}{2n_0^2} - \frac{m_ec^2\alpha^2z^2}{2} = -m_ec^2\alpha^2Z^2 = E_{1s^2}^{\mathrm{He}^0} = -78.975 \text{ eV} = -2.9 \text{ a.u.}, \quad (1)$$

i.e. the antiproton and the electron equally share the total binding energy, which in turn equals that of the capturing He^0 atom in the $1s^2$ ground state. For the effective charge, a value of $Z \approx 1.7$ follows from equation (1), in good agreement with a variational calculation by Russell [8].

In the neutral three-body Coulomb system thus formed the remaining electron stays essentially in the $1s$ ground state. The antiproton wavefunction in the initially populated state of antiprotonic helium should therefore considerably overlap that of the second electron, which would then be expected to be ejected rapidly *via* the Auger effect [9]. Due to the degeneracy of states of the resulting $\overline{p}\mathrm{He}^{2+}$ ion, the molecular potential between it (chemically resembling a heavy proton) and a colliding helium atom then induces fast Stark transitions of the antiproton to low-l states. These are immediately followed by its annihilation with the nucleus, resulting in an antiproton lifetime of the order of picoseconds. Applying laser spectroscopy techniques [10] to study the lifetimes and populations of individual states of $\overline{p}\mathrm{He}^+$ [11–16], we have shown that the "conventional" exotic atom cascade sketched above is ineffective for antiprotons captured into a class of circular or nearly circular states of antiprotonic helium with large orbital quantum numbers $l \lesssim n-1$, as was suggested earlier by Condo [17]. For these states the small energy level spacing of antiprotonic orbitals ($E_n - E_{n-1} \approx 2$ eV) requires a large jump in both n and l quantum numbers ($\Delta l > 3$) in order to release the energy necessary for ejection of the strongly bound remaining electron (≈ 24 eV). Since the Auger rate decreases by about three orders of magnitude as the multipolarity $|\Delta l|$ of the transition increases by one unit [10,18], these high-(n,l) states predominantly decay *via* a cascade of slow radiative dipole transitions with $\Delta l = \Delta n = 1$ or, equivalently, with constant vibrational quantum number $v = n - l - 1$, each with a lifetime of $\approx$ 1–2 μs [19,20]. Due to this strong dependence of the Auger rate on the multipolarity of the transition there is a distinct border between long-lived, radiation dominated states and short-lived states, where fast Auger transitions with $\Delta l \leq 3$ are energetically possible. The radiative cascade terminates when such a short-lived state is reached and the "normal" antiprotonic atom cascade *via* Auger and subsequent Stark transitions becomes effective, resulting in very fast (*i.e.* ps-scale) annihilation of the antiproton.

The metastable states of antiprotonic helium were investigated experimentally by measuring the time interval between the arrival of an antiproton at the helium target and its annihilation with a nucleon of the helium nucleus. Detailed studies of these delayed annihilation time spectra (DATS) showed that the anomalously long lifetime of antiprotons captured into metastable states in helium depends surprisingly little on the density or phase of the helium target and persists in high-density gas, liquid and even solid helium [5]. Even the admixture of the light noble gases neon, argon and krypton in concentrations of some 10% shortened the antiproton lifetime only slightly, without changing the overall cascade-dominated shape of the DATS [4,7]. Adding only 250 ppm of xenon gas, on the other hand, caused a noticeable decrease of the antiproton lifetime together with a significant change of the shape of the DATS [7].

A much stronger effect was observed when molecular gases were admixed to the helium target. While N_2 had an effect similar to xenon, a few hundred ppm of H_2 or O_2 molecules were sufficient to destroy the metastability almost completely [5]. From systematic investigations of DATS at various ppm-admixtures of H_2 and O_2 molecules, which revealed characteristic changes of their shape, we drew the conclusion that all the metastable states are destroyed with an efficiency independent of their quantum numbers in the case of O_2 [21], while the states are quenched in a highly state dependent way by H_2 [22].

In order to tag individual levels of this exotic three-body system, rather than study the integral effect of all metastable states involved in the cascade as reflected in the DATS, a laser spectroscopy technique was introduced [10]. This method is based on resonant deexcitation of the last metastable state in a given cascade to an adjacent short-lived Auger dominated state by irradiation with laser light of the corresponding wavelength. The resonance condition resulted in almost instantaneous annihilation of the antiproton and a spike-like response in the DATS at the time the laser was fired. Using this technique we were able not only to measure transition energies between highly excited states populated after antiprotonic helium formation, but also to determine their lifetimes as a function of the target conditions and foreign gas admixtures. In the case of H_2 admixtures, these laser spectroscopy measurements suggested that for a given cascade energetically higher-lying states are much more efficiently quenched than lower-lying ones. We have employed these state dependent quenching effects to selectively depopulate the higher one of two adjacent metastable levels in a cascade by adding an appropriate number density of H_2 molecules to the target gas and then applied a laser pulse to resonantly excite the $\overline{p}\mathrm{He}^+$ system from the long-lived lower level to the now short-lived upper one [23]. As in the pure helium case, an increased annihilation rate from the short-lived level was observed when the resonance condition was met.

In addition to providing a more systematic insight into the structure of metastable antiprotonic helium, this so-called "hydrogen-assisted inverse resonance" (HAIR) method offered the means to study the quenching effect by H_2 in greater detail [24]. The quenching cross-sections obtained for a variety of six metastable states with this technique yielded important information on the n and l

dependence of the H_2 quenching of states, showing that within a given cascade with constant vibrational quantum number v, the quenching cross-section increases by a factor of 4–6 when n increases by one, while it decreases moderately with increasing l.

In order to shed some new light on the physics of the underlying quenching processes, it was evidently necessary to investigate the influence of the different vibrational and rotational level structure of deuterium molecules on the quenching efficiency. In the present paper we first give a brief description of the experimental arrangements used for our measurements. The subsequent comparison of DATS with H_2 and D_2 admixtures can only give a qualitative picture of the quenching, which is then put on a quantitative basis by using laser spectroscopy techniques to measure the lifetimes of individual states or cascades and to deduce H_2 and D_2 quenching cross-sections for the states $(39, 35)$ and $(37, 34)$.

2 Experiment

The experiments on antiprotonic helium were performed at the Low Energy Antiproton Ring (LEAR) of CERN using a 200 MeV/c antiproton beam (momentum spread 0.1%), which was extracted from the ring in two different modes: (i) continuous, "slow" extraction at a rate of about $10^4\,\overline{p}$/s, and (ii) pulsed, "fast" extraction of 100–200 ns long bunches, each containing about $10^8\,\overline{p}$.

Figure 1(top) shows a perspective view of the experimental setup during slow extraction of the antiprotons from LEAR. After the end of the beamline, a 100 μm thick Be window, the antiproton beam traversed a few cm of air and passed a 0.45 mm plastic scintillation counter, which provided the start signal for the annihilation time measurement (not shown in Fig. 1). It entered the target chamber through Kapton and CuBe windows and was stopped in a cylindrical helium gas target, which was kept at cryogenic temperatures by a cold helium gas-flow cryostat. The dye laser pulse, which was expanded by lenses to cover the $\overline{p}$ stopping region in the target vessel, was introduced through quartz windows on the side opposite to the beam entrance windows. The annihilation time of each stopped antiproton was measured by seven scintillator-lead shower counters, which detected at least two of an average of five annihilation pions with an efficiency of $(99.7 \pm 0.1)\%$ [25]. This multiplicity requirement was necessary to eliminate the background caused by the $\pi^+ \to \mu^+ \to e^+$ decay chain of positive annihilation pions stopped in the vicinity of the target. This way, DATS essentially free of background could be recorded, as shown in Figure 2.

For laser spectroscopy experiments, however, the intrinsic ignition time of the laser system, which was triggered by a randomly arriving antiproton, imposed a lower limit of 1.3 μs on the earliest possible time to study individual metastable states – too late for a proper investigation of certain quenching phenomena. This constraint could be overcome in the pulsed antiproton extraction mode, where the signal that initiated the extraction was used to trigger the laser system in advance of the arrival of the $\overline{p}$ bunch, thus bypassing the delay caused by the ignition of the laser. In the pulsed mode, however, it was evidently not possible to resolve individual annihilations of about 3×10^6 antiprotons occurring within some 10 μs. Therefore, the shower counters were replaced by a single Lucite radiator placed on one side of the target vessel (Fig. 1(bottom)), the Čerenkov light pulse produced by the charged annihilation products therein being detected by a highly linear, gated photomultiplier tube (PMT HAMAMATSU R5504GX-ASSY). The pulse time evolution was recorded by a 500 MHz (2 GSa/s) digital

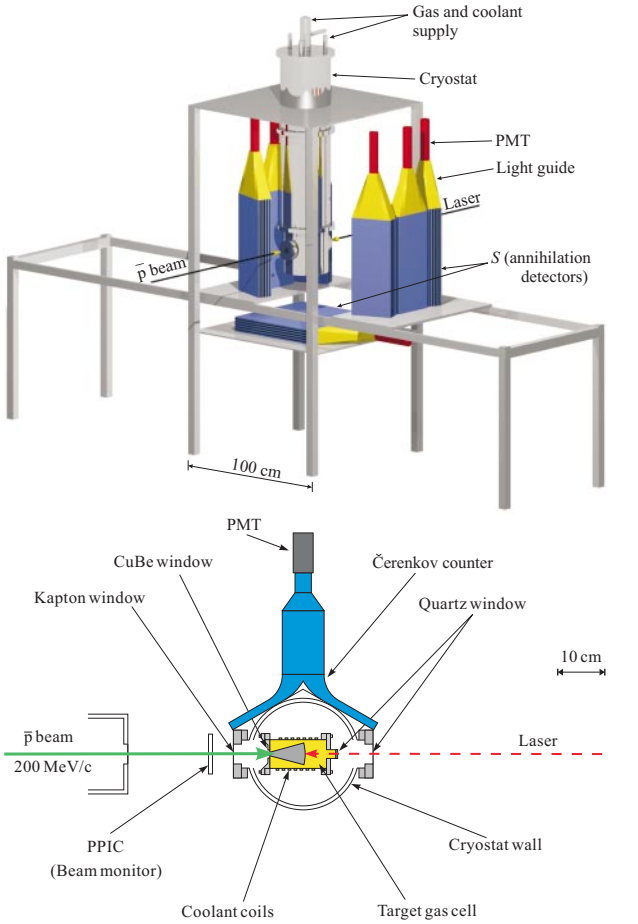

Fig. 1. (top) Perspective view of the experimental arrangement during slow extraction of the antiprotons from LEAR. A beam of $\approx 10^4\,\overline{p}$/s (momentum 200 MeV/$c$) passed a scintillation counter telescope (not shown) and entered the target chamber through Kapton and CuBe windows, where it was stopped in cold helium gas. The laser beam was introduced through quartz windows on the side opposite to the beam windows. (bottom) Plan view of the setup used in the pulsed extraction mode. The shower counters of (top) were replaced by a Lucite radiator, the Čerenkov light produced therein by the charged annihilation pions being detected by a gated PMT. A parallel plate ionization chamber (PPIC) was used instead of the scintillator telescope to monitor the position and the time structure of the beam.

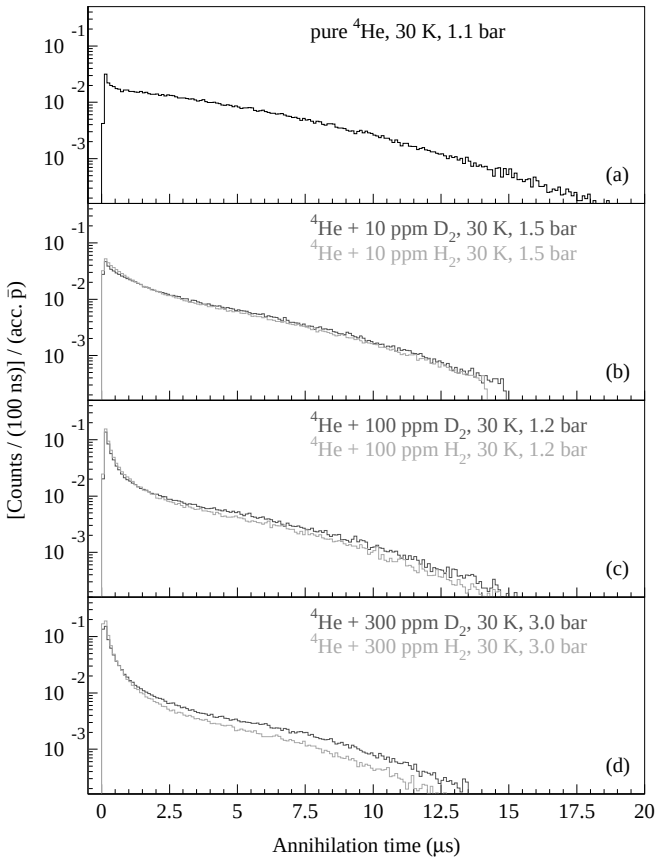

Fig. 2. Delayed annihilation time spectra (a) in pure helium and (b–d) at various number densities of H_2 (grey line) and D_2 (black line) molecules, obtained by varying the admixture ratio as well as the target pressure. For a proper comparison the DATS were normalized to the number of accepted antiprotons, *i.e.* the total number of events in the spectrum. In order to increase the data taking rate, the time window was reduced to $\approx 15\,\mu$s for the measurements (b–d), which caused the abrupt cutoff of the spectrum in (b). For (c) and (d) the maximum antiproton lifetime was already shorter than the time window.

oscilloscope. This analog detection method, however, did not permit the $2.2\,\mu$s background caused by the decay chain of π^+ to be suppressed. This fact could be accounted for in laser spectroscopy experiments [24], where either the intensity of a resonance spike or its shape play a role, but it ruled out the analysis of full DATS recorded during fast extraction.

The target consisted of ^{4}He (purity > 99.9999%) for the measurements in pure helium, and of several samples of ^{4}He (purity > 99.9996%) to which H_2 (purity > 99.999%) and D_2 (purity > 99.7%) had been premixed to the desired concentrations, and the composition of which had been analyzed by the supplier with a relative accuracy of 2%. To exclude the possibility of contamination by impurities such as O_2 or N_2 the target gas was kept at a temperature of 30 K throughout the experiment, well above the boiling temperatures of H_2 (20.3 K) and D_2 (23.7 K) [26]. The absolute number density of H_2 and D_2 molecules in the target gas was controlled by varying the pressure of the gas samples between 1 bar and 10 bar. The various temperature, pressure and H_2 or D_2 admixture conditions for the different measurements are given in Tables 1 and 2.

3 DATS with H_2 and D_2 admixtures

For a comparison of the overall quenching efficiency of H_2 and D_2 molecules we measured a series of DATS at various H_2 and D_2 admixture ratios without laser irradiation, as shown in Figure 2. Here, only the delayed part of the spectrum (annihilation time $\gtrsim 80$ ns) is shown, while the peak of prompt annihilating antiprotons has been cut off by an electronic veto. When plotted in a semilogarithmic scale, the DATS in pure ^{4}He (Fig. 2a) exhibits the typical downward bent structure, which reflects the effect of parallel $\overline{p}$ cascades over several adjacent metastable levels. The small fast-decaying component at early times appears at helium target densities above 4×10^{-4} mol/cm^3. Its decay rate gradually increases with increasing density, until it is fully absorbed into the prompt peak at a target density of 12×10^{-4} mol/cm^3 [27]. While the appearance of a second short-lived component at densities higher than 15×10^{-4} mol/cm^3 has been attributed to the density dependent lifetime shortening of a single metastable state with quantum numbers $(n, l) = (37, 34)$ [27], the origin of the fast-decaying component present in Figure 2a has not yet been clarified. Figures 2b–2d show DATS recorded at H_2 and D_2 admixture ratios of (b) 10 ppm at 1.5 bar, (c) 100 ppm at 1.2 bar and (d) 300 ppm at 3.0 bar, corresponding to number densities of foreign gas molecules of (b) 0.36×10^{16} cm^{-3}, (c) 2.9×10^{16} cm^{-3} and (d) 21.7×10^{16} cm^{-3}, respectively. Obviously, the characteristic behavior of the DATS as D_2 molecules are added is very similar to the case of H_2 admixtures: certain long-lived states are converted to shorter-lived ones, resulting in an increasing short-lived component and a decreasing long-lived part with increasing number density of foreign gas molecules. The fact that the cascade-governed growth-decay structure persists even at high admixture ratios shows that the quenching of states is strongly non-uniform both for H_2 and D_2 molecules. This behavior is in strong contrast to the case of O_2 admixtures, where a single exponential decay indicates that the quenching efficiency by O_2 molecules is similar for all metastable levels [21]. In evaluating the significance of the slightly shorter overall antiproton lifetime in the case of H_2 admixtures compared to the corresponding D_2 concentration, the different thermal velocities of the H_2 and D_2 molecules must of course be taken into account, as we have done in equations (2, 3) below.

4 Effect of H_2 and D_2 on individual metastable states

Since the DATS reflect the integral effect of several $\overline{p}$ cascades over many metastable levels, no information concerning the effect of H_2 and D_2 admixtures on individual

Table 1. Inverse cascade lifetimes $(T_v)^{-1}$ and decay rates γ of the last metastable levels in the cascades $v = 2$ and $v = 3$ as a function of target gas temperature T, pressure p and concentration of H_2 molecules c_{H_2}. Quantities derived therefrom are the molar density of helium atoms ρ_{mol} and the number density of H_2 molecules n_{H_2}. For the measurements in pure helium, the upper limit of the H_2 content as certified by the supplier is given. The errors in T and p take into account the experimental uncertainty of the sensors as well as slow variations in time due to the varying heat load by the laser and other external sources.

T (K)	p (bar)	ρ_{mol} (10^{-4} mol/cm^3)	c_{H_2} (ppm)	n_{H_2} (10^{16} cm^{-3})	decay rate (μs^{-1})
		slow extraction			$(T_{v=2})^{-1}$
29.4(6)	1.160(12)	4.74(10)	9.90(20)	0.282(8)	0.592(16)
29.3(5)	1.263(19)	5.17(11)	30.0(6)	0.934(27)	0.752(22)
29.53(5)	1.243(13)	5.05(9)	98.6(20)	3.00(9)	1.01(5)
29.22(5)	1.190(10)	4.89(9)	291(6)	8.57(23)	1.44(11)
29.77(4)	1.148(9)	4.63(7)	968(20)	27.0(7)	4.2(13)
		pulsed extraction			$(T_{v=2})^{-1}$
100.0(5)	4.109(21)	4.91(4)	≤ 0.5	≤ 0.015	0.427(27)[a]
		slow extraction			$(T_{v=2})^{-1}$
30.18(3)	2.926(21)	11.61(14)	≤ 0.5	≤ 0.035	0.481(18)
30.1(7)	2.94(3)	11.68(29)	9.90(20)	0.696(23)	0.883(29)
30.2(4)	2.957(26)	11.72(16)	98.6(20)	6.96(17)	1.61(12)
32.1(29)	3.12(26)	11.6(15)	291(6)	20.4(25)	2.3(7)
		pulsed extraction			$(T_{v=2})^{-1}$
30.40(10)	3.086(17)	12.16(8)	≤ 0.5	≤ 0.037	0.491(17)
31.00(10)	3.060(16)	11.82(7)	9.90(20)	0.705(15)	0.855(23)
30.00(10)	3.020(16)	12.06(8)	30.0(6)	2.18(5)	1.01(4)
30.00(10)	3.037(16)	12.12(8)	98.6(20)	7.20(15)	1.53(5)
29.30(10)	3.033(16)	12.40(8)	291(6)	21.7(5)	2.50(10)
29.94(14)	3.009(17)	12.04(9)	968(20)	70.2(15)	6.67(29)
		slow extraction			$\gamma(37, 34)$
6.35(5)	0.251(5)	4.85(9)	≤ 0.5	≤ 0.015	0.90(6)[b]
29.0(11)	1.157(21)	4.78(21)	9.90(20)	0.285(14)	0.88(5)
29.5(5)	1.256(19)	5.11(11)	30.0(6)	0.924(27)	1.00(4)
29.83(21)	1.204(7)	4.85(5)	98.6(20)	2.88(7)	1.12(10)
29.2(5)	1.191(10)	4.90(9)	291(6)	8.59(23)	1.49(16)
29.8(4)	1.148(9)	4.63(7)	968(20)	27.0(7)	2.7(13)
30.0(10)	2.87(6)	11.5(5)	≤ 0.5	≤ 0.035	1.04(6)
30.2(7)	2.94(3)	11.69(29)	9.90(20)	0.697(23)	1.22(6)
30.1(26)	2.92(29)	11.6(14)	98.6(20)	6.9(8)	1.50(9)
30.8(21)	3.07(19)	12.0(11)	291(6)	21.0(20)	2.9(6)
		slow extraction			$(T_{v=3})^{-1}$
30.24(24)	1.555(9)	6.17(6)	9.90(20)	0.368(9)	1.33(18)
		pulsed extraction			$(T_{v=3})^{-1}$
30.06(11)	3.058(17)	12.18(8)	≤ 0.5	≤ 0.037	0.509(14)
30.00(10)	3.094(16)	12.35(8)	9.90(20)	0.736(16)	1.97(7)
29.90(10)	3.043(16)	12.19(8)	30.0(6)	2.20(5)	5.0(4)
30.00(10)	3.029(16)	12.09(8)	30.0(6)	2.18(5)	5.4(4)
30.00(10)	3.040(16)	12.14(8)	98.6(20)	7.21(15)	21(8)
		slow extraction			$\gamma(39, 35)$
5.80(5)	0.550(5)	12.12(17)	≤ 0.5	≤ 0.037	0.644(15)[c]
30.7(7)	1.571(19)	6.13(15)	9.90(20)	0.366(12)	1.5(4)

[a]Measured at 100 K and 4.1 bar [21], *i.e.* at a density equal to that during the measurements at 30 K and 1.2 bar. [b]Interpolated from measurements on the density dependence of $\gamma(37, 34)$ in pure helium at 6.3 K [27]. [c]From measurements on the density dependence of $\gamma(39, 35)$ in pure helium, which showed that the lifetime of this state remains constant over a wide range of densities up to supercritical helium [27].

Table 2. Inverse cascade lifetimes $(T_v)^{-1}$ and decay rates γ of the last metastable levels in the cascades $v = 2$ and $v = 3$ for various number densities of D_2 molecules n_{D_2}. For the definition of the other quantities see Table 1.

T (K)	p (bar)	ρ_{mol} (10^{-4} mol/cm^3)	c_{D_2} (ppm)	n_{D_2} (10^{16} cm^{-3})	decay rate (μs^{-1})
		slow extraction			$(T_{v=2})^{-1}$
30.18(28)	2.926(21)	11.61(14)	≤ 0.5	≤ 0.035	0.481(18)
30.4(15)	2.93(8)	11.5(7)	105.8(22)	7.4(5)	1.18(8)
30.52(21)	3.035(16)	11.90(11)	313(7)	22.4(5)	1.74(22)
30.52(21)	3.045(18)	11.94(11)	313(7)	22.5(5)	1.70(14)
		pulsed extraction			$(T_{v=2})^{-1}$
30.40(10)	3.086(17)	12.16(8)	≤ 0.5	≤ 0.037	0.491(17)
30.06(11)	3.053(17)	12.17(8)	9.85(30)	0.722(23)	0.684(20)
30.30(10)	3.030(16)	11.98(8)	30.7(10)	2.21(7)	0.957(20)
30.00(10)	3.031(16)	12.10(8)	105.8(22)	7.71(17)	1.229(23)
30.29(11)	3.035(16)	12.00(8)	1033(21)	74.6(16)	3.84(21)
		slow extraction			$\gamma(37, 34)$
30.0(10)	2.87(6)	11.5(5)	≤ 0.5	≤ 0.035	1.04(6)
30.4(15)	2.93(8)	11.5(7)	105.8(22)	7.4(5)	1.40(24)
30.8(28)	3.1(16)	11.9(12)	313(7)	22.3(23)	1.41(13)
		pulsed extraction			$(T_{v=3})^{-1}$
30.06(11)	3.058(17)	12.18(8)	≤ 0.5	≤ 0.037	0.509(14)
30.08(22)	3.060(21)	12.18(13)	9.85(30)	0.722(24)	1.93(5)
30.19(22)	3.038(16)	12.05(11)	30.7(10)	2.23(7)	4.31(17)
		slow extraction			$\gamma(39, 35)$
5.80(5)	0.550(5)	12.12(17)	≤ 0.5	≤ 0.037	0.644(15)[a]
29.8(21)	1.48(7)	6.0(5)	9.85(30)	0.35(4)	1.00(22)
30.33(15)	1.007(6)	3.99(3)	30.7(10)	0.737(23)	2.7(12)

[a] From measurements on the density dependence of $\gamma(39, 35)$ in pure helium, which showed that the lifetime of this state remains constant over a wide range of densities up to supercritical helium [27].

states or possible isotope effects can be gained from an investigation of DATS alone. Therefore we applied the laser resonance method to measure the lifetime shortening of the states $(n, l) = (37, 34)$ at the end of the cascade $v = 2$ and $(39, 35)$ at the end of the cascade $v = 3$ at various H_2 and D_2 admixture ratios. First results from the analysis of a small data set for the case of H_2 admixtures alone have already been reported in [22]. From these measurements we had concluded that for the cascades $v = 2$ and $v = 3$ states with higher n are much more strongly quenched by collisions with H_2 molecules than those with lower n. This observation provided the basis for the HAIR technique [23]. Here, we present the results for both H_2 and D_2 admixtures obtained after the final analysis of all available data.

4.1 Determination of level lifetimes

We developed several methods, partly complementing each other, to measure the lifetimes of individual metastable states. Two of them, the "depletion recovery method" and the "overall cascade lifetime method", provided the basis for the results reported in this paper and will be described briefly in the following.

The lifetimes of the two levels involved in a laser induced transition between a metastable level and an adjacent short-lived one at the end of a given cascade can be determined directly by studying the pulse shape of the resonance spike and the depletion zone following the spike in the DATS. In particular, it can be shown that the dip in the DATS caused by laser-induced annihilations which are then missing after the spike, recovers to the shape of DATS without laser irradiation with a time constant determined only by the decay rate of the resonantly deexcited state [27]. Figure 3 shows the depletion-recovery spectrum, *i.e.* the difference between the normalized DATS with and without laser irradiation, obtained (a) in pure helium and (b) at an H_2 admixture of 100 ppm with the laser on resonance with the transition $(37, 34) \rightarrow (36, 33)$ at 470.72 nm. The insets display an enlarged view of the peak area together with a fit of a sum of two exponentials, describing the peak decay and the depletion recovery, respectively. The decay rate γ of the level $(37, 34)$ obtained this way is noted for both cases, clearly showing the lifetime shortening of the $(37, 34)$ state by H_2 admixtures.

The state emptied by the laser is repopulated from higher-lying states, an effect which can be studied by

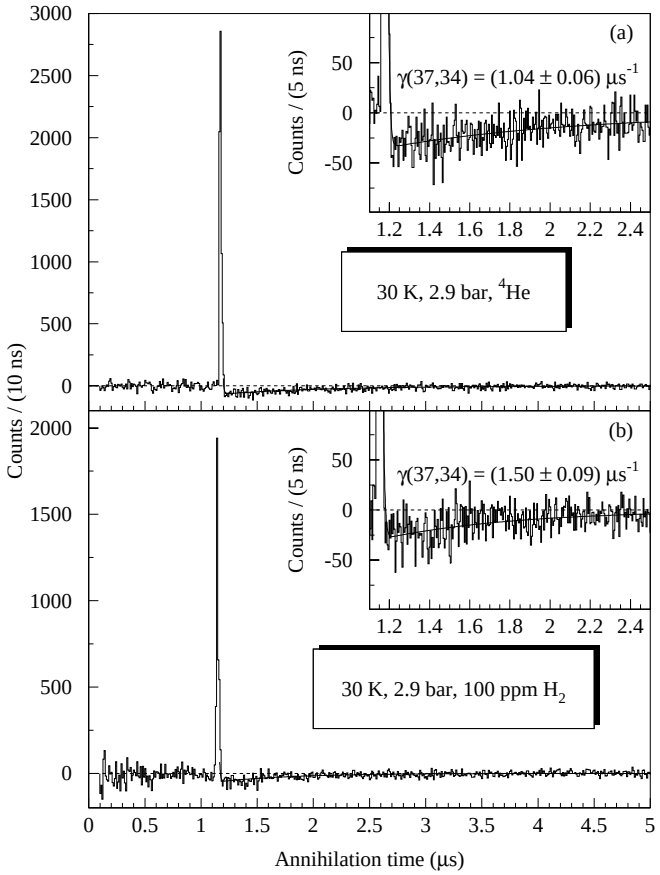

Fig. 3. Depletion-recovery spectrum of the 470.72 nm resonance at 30 K, 2.9 bar (a) in pure helium and (b) at an H_2 admixture of 100 ppm, together with a fit of a sum of two exponentials describing the peak decay and the depletion recovery, respectively.

varying the laser firing time with respect to the arrival of the antiproton, as shown for the 470.72 nm resonance in Figure 4 for (a–d) slow and (e–h) fast extraction modes. The advantage of a much earlier laser firing time in fast extraction mode (due to the accelerator signal preceding $\overline{p}$ extraction) is clearly visible. The resonance intensity reflects the time evolution of the population in the resonantly deexcited level, which is determined not only by its own lifetime, but also by its repopulation from higher-lying levels in the same cascade. When plotted against the laser firing time, the resonance intensity exhibits an approximately single exponential decay with a lifetime T_v, the so-called "overall cascade lifetime". Figure 5 shows the dependence of the resonance intensity on the laser firing time for the measurements during (a) slow and (b) fast extraction shown in Figure 4. For the event-wise acquisition applied in the slow extraction mode of (a), the resonance intensity was determined by subtracting DATS without laser irradiation, which were recorded simultaneously to those with laser light during the dead time of the laser, from DATS with laser, both normalized to the same number of entries before the resonance peak (see the enlarged insets in Figs. 4a–4d). The number of entries in the resonance peak above background was then normalized to the total number of events in the DATS between 0.1 μs and 5 μs to yield the resonance intensities plotted in Figure 5a. Since the DATS recorded in fast extraction are the result of only a single laser pulse, there was no simultaneous recording of DATS without laser irradiation. Consequently, the resonance intensity was determined by fitting a single exponential to a 60 ns wide range before and after the laser peak, respectively (see insets in Figs. 4e–4h) and subtracting this function from the analog DATS. The resonance intensity plotted in Figure 5b is then calculated from the area under the laser peak above background, normalized to the total area between 0.3 μs and 10 μs. The overall cascade time deduced by fitting a single exponential to the decay of the resonance intensity is also indicated in Figure 5, showing that the results obtained in fast extraction agree very well with those from slow extraction.

In contrast to DATS recorded event by event in slow extraction, where the assignment of error bars is straightforward, an analog DATS obtained in fast extraction reflects the time evolution of a single light pulse produced by the charged annihilation products of some 10^8 $\overline{p}$ stopped in the target. Generally, the error of the observed signal amplitude is then given by the statistical fluctuations of the number of annihilation events and the pulse height fluctuations of a single annihilation event. Here, the bin errors were determined from an analysis of the statistical deviations of each measured DATS from its expected smooth, multi-exponential decrease. The error bars determined therefrom are in good agreement with an estimate of the errors taking into account the various physical processes from Čerenkov light production to photoconversion in the PMT [24].

4.2 Lifetime shortening by H_2

First we applied the techniques described above to the transition $(37, 34) \rightarrow (36, 33)$ in the cascade $v = 2$ at a vacuum wavelength of 470.72 nm, which had previously been studied extensively in pure helium [12,27], at various H_2 admixture rates. In Figure 6a the cascade lifetime $T_{v=2}$ is presented together with the lifetime $\tau(37, 34)$ of the last metastable state at a temperature of 30 K and a pressure of 3 bar as a function of the number density of H_2 molecules n_{H_2}. The corresponding concentration of H_2 molecules is given at the top abscissa. The fact that $T_{v=2}$ is about a factor of two larger than $\tau(37, 34)$ in pure helium reflects the feeding of the state emptied by the laser from higher-lying levels in the same cascade. With increasing H_2 concentration this feeding gradually decreases and can be neglected completely above 100 ppm, corresponding to a number density of H_2 molecules of about 8×10^{16} cm^{-3}. At these conditions the resonance intensity of the 470.72 nm transition decreases according to the lifetime of the last metastable level, so that the cascade lifetime can be interpreted as the lifetime of the last metastable state. A completely analogous behavior had

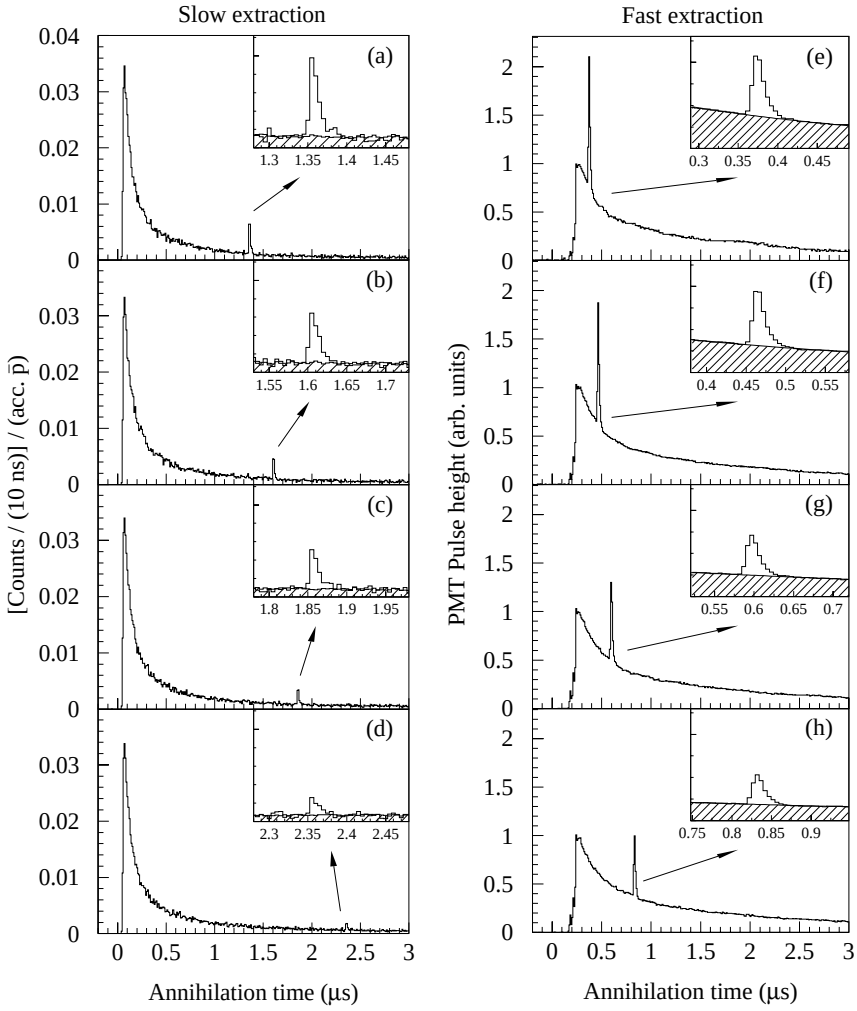

Fig. 4. Series of DATS obtained in (a–d) slow extraction (normalized to the number of accepted $\overline{p}$) and (e–h) fast extraction of antiprotons, recorded at a target gas temperature of 30 K and a pressure of 3 bar. The resonance intensity of the transition $(37, 34) \rightarrow (36, 33)$ at 470.72 nm reflects the time evolution of the population of the resonantly deexcited level $(37, 34)$ at an H_2 admixture of 100 ppm. The hatched background areas in the insets correspond to DATS recorded without laser irradiation in the slow extraction cases (a–d) and to fits of a single exponential to the fast extraction spectra (e–h).

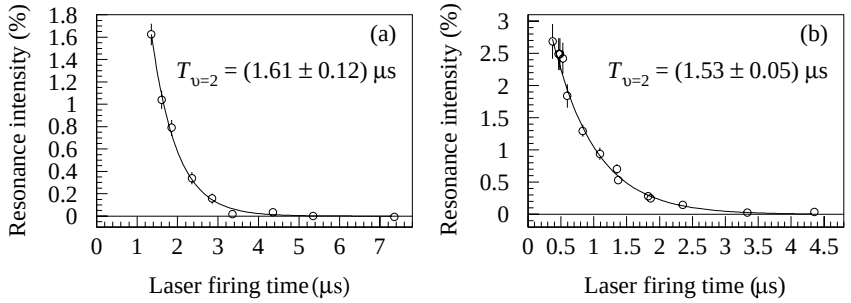

Fig. 5. Resonance intensity of the 470.72 nm transition *versus* laser firing time, from measurements during (a) slow extraction and (b) fast extraction of antiprotons at 30 K, 3 bar and an H_2 admixture of 100 ppm.

been found previously from an analysis of a subset of the present data at a target gas pressure of 1.2 bar [23]. Due to the density dependent shortening of the lifetime $\tau(37, 34)$ in pure helium mentioned above, the lifetimes measured at 3 bar are shifted towards smaller values compared to the ones at 1.2 bar. Table 1 summarizes all experimental results for the inverse cascade lifetime $(T_{v=2})^{-1}$ and for the decay rate $[\tau(37, 34)]^{-1} \equiv \gamma(37, 34)$ as a function of temperature T, pressure p and number density n_{H_2} of H_2 molecules.

A qualitatively similar picture, but shifted to much lower H_2 concentrations, resulted from the observation of the transition $(39, 35) \rightarrow (38, 34)$ in the cascade $v = 3$ at a laser wavelength of 597.26 nm. As can be seen from Figure 6b, the cascade lifetime $T_{v=3}$ approached the lifetime $\tau(39, 35)$ of the last metastable level already at an H_2 admixture ratio of 10 ppm. At 30 ppm the lifetime of the resonantly deexcited level was too short for the resonance to be observed in the slow extraction mode. In this case the cascade lifetimes measured in the pulsed extraction mode yielded directly the lifetime $\tau(39, 35)$ of the

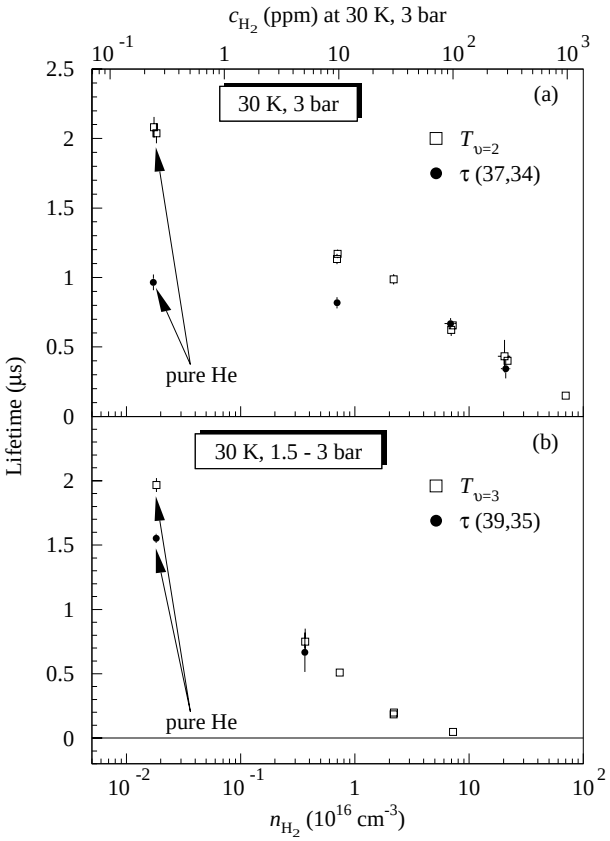

Fig. 6. Cascade lifetime T_v (open squares) of the cascades (a) $v = 2$ and (b) $v = 3$ as a function of the number density n_{H_2} of H_2 molecules (bottom abscissas) or the H_2 concentration (upper abscissa), compared with the respective lifetime $\tau(n, l)$ of the last metastable state in the corresponding cascade (full circles). The data points in pure helium (H_2 impurity content $\leq$ 0.5 ppm) are plotted at an H_2 concentration of 0.25 ppm. Since the lifetime of the state $(39, 35)$ is known to remain constant over a wide range of densities [27], data points at different target densities were taken into account for (b).

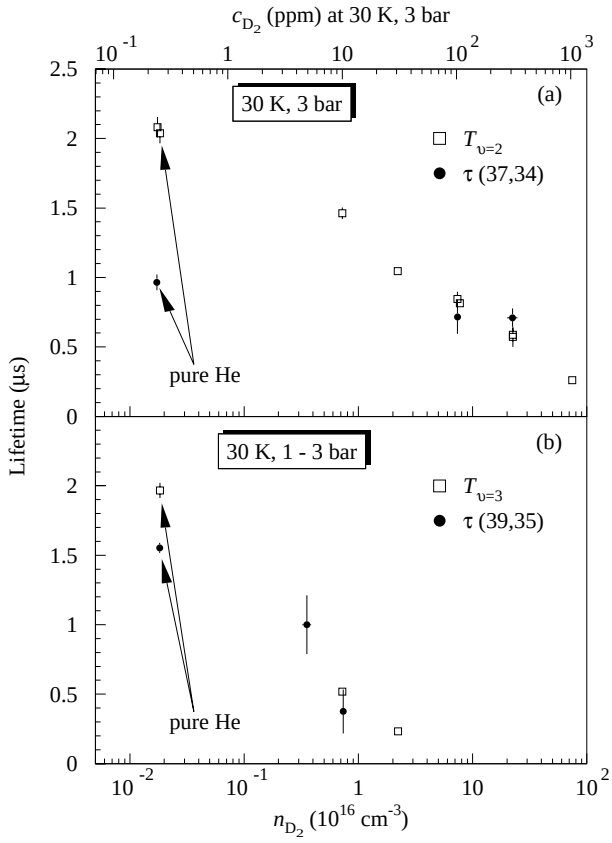

Fig. 7. Same as Figure 6 for D_2 admixtures.

last metastable level. All available experimental results for the inverse lifetime $(T_{v=3})^{-1}$ as well as the decay rate $\gamma(39, 35)$ of the state $(39, 35)$ at different temperatures, pressures and H_2 admixture ratios are given in Table 1.

4.3 Lifetime shortening by D_2

In order to look for possible isotope differences in the quenching of metastable states by H_2 and D_2 admixtures, we performed a sequence of similar measurements for D_2 admixtures. The results for $T_{v=2}$ and $\tau(37, 34)$ measured at various D_2 admixture ratios at 30 K and 3 bar are shown in Figure 7a. As in the case of H_2 admixtures, the feeding from higher-lying states diminishes with increasing D_2 concentration. Above a number density of 1×10^{17} cm^{-3}, there is no repopulation of the state $(37, 34)$ after its emptying by the laser, so that its lifetime $\tau(37, 34)$ is equivalent to the cascade lifetime $T_{v=2}$ as measured by varying the laser firing time. The experimental values for the decay rates in the cascade $v = 2$ measured at different D_2 concentrations are summarized in Table 2.

Similar measurements for the transition $(39, 35) \rightarrow (38, 34)$ at 597.26 nm confirm also for D_2 admixtures that the higher-lying state $(39, 35)$ is subject to a much stronger quenching, as can be seen from Figure 7b. The results for $(T_{v=3})^{-1}$ and $\gamma(39, 35)$ obtained at various experimental conditions are given in Table 2.

4.4 Quenching cross-sections

Before we started employing laser spectroscopy to study the metastable states of antiprotonic helium, two possible mechanisms responsible for the hydrogen-induced shortening of the antiproton lifetime in helium had to be considered. Either the initial population of metastable states was reduced due to a modified energy distribution of antiprotons before capture, or the lifetime of already populated metastable states was shortened. The fact observed earlier that the fraction of delayed annihilations remained nearly constant, independent of the foreign gas concentration [3], already provided a strong indication for the latter. The lifetime measurements of individual states reported in this paper undoubtedly confirm this conjecture.

The fact that the decay rates of all the states under investigation exhibit a linear increase with increasing number density of H_2 or D_2 molecules suggests

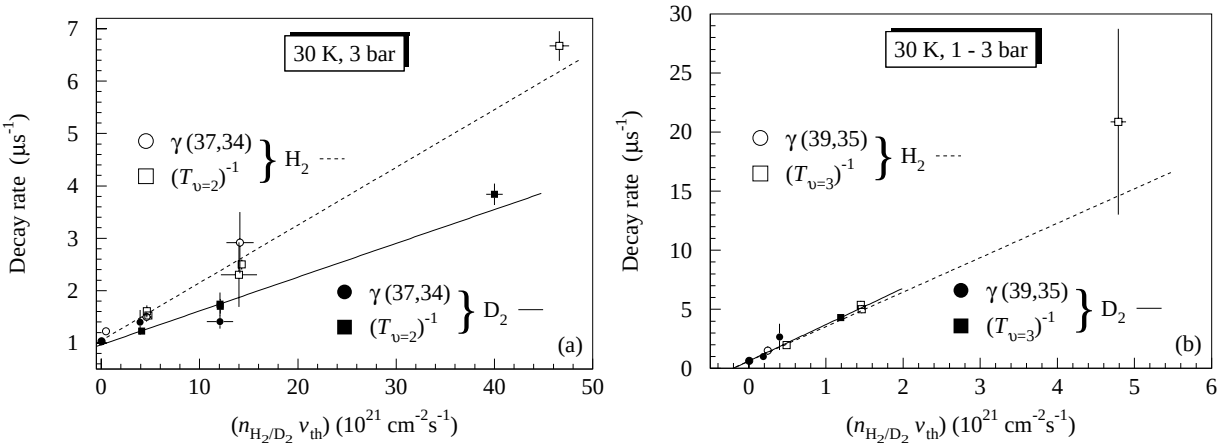

Fig. 8. Decay rates of the levels (a) $(37, 34)$ and (b) $(39, 35)$ at various H_2 (empty symbols) and D_2 admixtures (filled symbols).

a simple model, in which the metastable states are depopulated in binary collisions with foreign gas molecules X_2. The observed non-uniform quenching of states is accounted for by a state dependent quenching cross-section $\sigma_q^{X_2}(n,l)$, averaged over the distribution of thermal velocities at 30 K. The experimental decay rate $\gamma(n,l)$ of a given level is then determined by the decay rate in pure helium, $\gamma_0(n,l)$, and the collisional depopulation rate, $\gamma_q^{X_2}(n,l) = n_{X_2} v \sigma_q^{X_2}(n,l)$, where n_{X_2} denotes the number density of foreign gas molecules and v is the relative velocity of the collision partners. Since the thermalization time of the $\overline{p}He^+$ system, which immediately after formation has a kinetic energy of the order of some eV, is much shorter than the typical lifetimes of metastable states [28], we assume thermal equilibrium when a foreign gas molecule is encountered. The total decay rate of a state (n,l) is then given by

$$\gamma(n,l) = \gamma_0(n,l) + n_{X_2} v_{th} \sigma_q^{X_2}(n,l), \qquad (2)$$

with the thermal relative velocity [29]

$$v_{th} = \sqrt{\frac{8 k_B T}{\pi M}}. \qquad (3)$$

Here, k_B is the Boltzmann constant, T the target gas temperature and M the reduced mass of the $\overline{p}He^+$–X_2 system. At a temperature of 30 K, v_{th} is 660 m/s for a $\overline{p}He^+$–H_2 collision and 530 m/s for a $\overline{p}He^+$–D_2 collision.

In Figure 8 we compare the experimental decay rates of the levels (a) $(n,l) = (37, 34)$ and (b) $(39, 35)$ for various number densities of H_2 (open symbols) and D_2 (full symbols) molecules. To account for small temperature fluctuations during the individual measurements, the results are plotted *versus* the areal collision rate $n_{H_2/D_2}(T)\, v_{th}(T)$ (in units of cm^{-2}s^{-1}) of the $\overline{p}He^+$ system with foreign gas molecules. The circles indicate results obtained with the depletion-recovery analysis, which directly yields the decay rate of the level under consideration, while the squares denote inverse average cascade lifetimes determined by varying the laser firing time. According to our discussion in the previous section, these can be interpreted as the decay rate of the last metastable level, provided that repopulation of the state is negligible.

Table 3. Cross-sections $\sigma_q(n,l)$ for the quenching of antiprotonic helium atoms by H_2 and D_2 admixtures as obtained from the fit of equation (2) to the experimental results for the decay rates of the levels $(39, 35)$ and $(37, 34)$.

(n,l)	$\sigma_q^{H_2}$ (10^{-16} cm^2)	$\sigma_q^{D_2}$ (10^{-16} cm^2)
$(39, 35)$	29.2(11)	30.8(14)
$(37, 34)$	1.10(5)	0.65(5)

From a fit of equation (2) to $\gamma(37, 34)$ with H_2 admixtures (Fig. 8a, dashed line), a quenching cross-section of $\sigma_q^{H_2}(37, 34) = (1.10 \pm 0.05) \times 10^{-16}$ cm^2 was obtained. In the case of D_2 admixtures (Fig. 8a, full line), a quenching cross-section for this level of $\sigma_q^{D_2}(37, 34) = (0.65 \pm 0.05) \times 10^{-16}$ cm^2 follows from the fit.

For the level $(n,l) = (39, 35)$ we deduced a quenching cross-section by H_2 molecules of $\sigma_q^{H_2}(39, 35) = (29.2 \pm 1.1) \times 10^{-16}$ cm^2. The decay rates $\gamma(39, 35)$ with D_2 admixtures yield a cross-section of $\sigma_q^{D_2}(39, 35) = (30.8 \pm 1.4) \times 10^{-16}$ cm^2, a value which agrees with the H_2 result within the error bars.

Table 3 summarizes the results for the quenching cross-sections of the levels $(37, 34)$ and $(39, 35)$ by H_2 and D_2 molecules.

5 Discussion and conclusions

Our laser spectroscopy experiments on antiprotonic helium confirm the conjecture of a similar quenching efficiency of hydrogen and deuterium molecules, which had been suggested already by the measurements of DATS without laser irradiation. The strong dependence of the quenching cross-section on the principal quantum number n observed in the case of H_2 seems to be even more pronounced in the case of D_2 admixtures: for the state $(39, 35)$ we deduced H_2 and D_2 quenching cross-sections which are

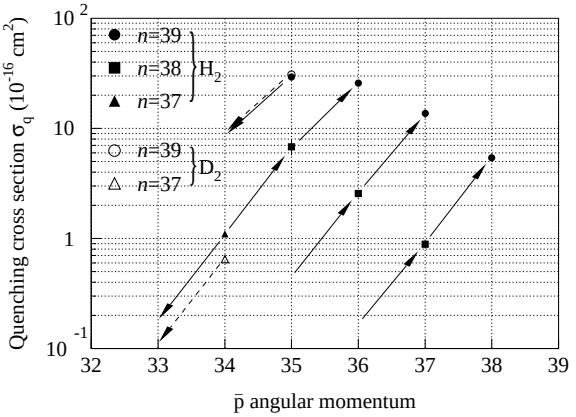

Fig. 9. Dependence of the quenching cross-sections by H_2 (full symbols) and by D_2 (open symbols) on the quantum numbers n and l. Arrows pointing downwards indicate laser induced transitions between a metastable and a short-lived, Auger-dominated level, while those pointing upwards represent HAIR transitions between a long-lived lower and an H_2-induced short-lived upper level.

equal within the errors, while for the lower lying state $(37, 34)$ we found that the quenching cross-section for D_2 is smaller than the H_2 value by a factor of (1.7 ± 0.2). Our current knowledge about the n- and l-dependence of the quenching by H_2 and D_2 molecules, including results obtained from HAIR measurements for the levels $(38, l)$, $l = 35, 36, 37$ and $(39, l)$, $l = 36, 37, 38$ [24], is summarized in Figure 9.

Possible mechanisms leading to an enhanced depopulation of metastable levels in collisions with foreign gas molecules are inelastic collisions, which modify vibrational, rotational or electronic inner degrees of freedom of the collision partners, and reactive collisions, *e.g.* dissociation and ionization or exchange reactions. First preliminary results by Valiron *et al.* [30], who performed a calculation of the adiabatic electronic potential based on *ab initio* quantum chemistry techniques, indicate that the formation of an exotic molecule in the exchange reaction $\overline{p}\mathrm{He}^+ + \mathrm{H}_2 \rightarrow [(\overline{p}\mathrm{He}^+)\mathrm{H}] + \mathrm{H}$, which was suggested in [22], might provide a possible explanation of the observed phenomena. Considering that the $\overline{p}\mathrm{He}^+$ system chemically resembles a heavy hydrogen atom, the dynamics of this reaction is expected to be similar to that of the well-known $\mathrm{H} + \mathrm{H}_2 \rightarrow \mathrm{H}_2 + \mathrm{H}$ exchange reaction [31]. Indeed it was found that the potential barrier for the collision of the $\overline{p}\mathrm{He}^+$ system with an H_2 atom depends strongly on the geometrical conformation of nuclei during the approach (the conformations of a system are the different spatial arrangements of its nuclei or atoms, that cannot be made congruent by rotations), a fact well known for the collision of an H atom with an H_2 molecule. Averaging over all possible geometries and taking into account the modulation of the $\overline{p}$ orbit during the collision, Valiron *et al.* estimated n and l dependent reaction barriers which, if interpreted in terms of an Arrhenius-law, were in qualitative agreement with the observed systematics for the quenching cross-sections. In their model, the isotope effect on the quenching efficiency observed experimentally may arise from the different spatial extension of vibrational wave functions for H_2 and D_2 and from the change of the zero-point energy during the collision. Detailed calculations of rate constants and cross-sections taking into account resonance and tunnel effects, however, are still lacking and are eagerly awaited.

On the experimental side, further insight into the mechanism of state dependent quenching of levels by hydrogen and deuterium molecules can be gained by systematically studying the temperature dependence of the depopulation efficiency, with strong quenching of all levels to be expected at higher temperatures, when reaction barriers of the order of the thermal kinetic energy at 30 K, as estimated by Valiron, cease to play a role. In addition, the investigation of the quenching by D_2 can be easily extended to a wider range of metastable states employing the HAIR method. After the closure of LEAR in 1996, these experiments, however, have to wait for the Antiproton Decelerator (AD), an all-in-one machine to collect, store, cool and extract antiproton bunches currently being commissioned at CERN, to come into operation.

We are indebted to the LEAR and PS staff at CERN for their tireless dedication to providing us with the high-quality antiproton beam, to Dr. P. Valiron, Dr. J. Carbonell and S. Sauge for providing us with their preliminary theoretical results and to Hamamatsu Photonics Ltd. for developing the special gated PMT used in this experiment. The present work is supported by the German Bundesministerium für Bildung und Forschung, the Grants-in-Aid for Specially Promoted Research and for International Scientific Research of the Japanese Ministry of Education, Science and Culture, the Hungarian National Science Foundation and the Beschleunigerlaboratorium der Universität und Technischen Universität München. H.A.T. acknowledges the support of the Japan Society for the Promotion of Science.

References

1. F.J. Hartmann, in *Electromagnetic cascade and chemistry of exotic atoms*, edited by L.M. Simons, D. Horváth, G. Torelli (Plenum Press, New York, 1990).
2. M. Iwasaki *et al.*, Phys. Rev. Lett. **67**, 1246 (1991).
3. T. Yamazaki *et al.*, Nature **361**, 238 (1993).
4. S.N. Nakamura *et al.*, Phys. Rev. A **49**, 4457 (1994).
5. E. Widmann *et al.*, Phys. Rev. A **51**, 2870 (1995).
6. B. Ketzer *et al.*, Phys. Rev. A **53**, 2108 (1996).
7. E. Widmann *et al.*, Phys. Rev. A **53**, 3129 (1996).
8. J.E. Russell, Phys. Rev. A **1**, 721 (1970).
9. T.B. Day, Nouvo Cimento **18**, 381 (1960).
10. N. Morita, K. Ohtsuki, T. Yamazaki, Nucl. Instrum. Meth. Phys. Res. A **330**, 439 (1993).
11. N. Morita *et al.*, Phys. Rev. Lett. **72**, 1180 (1994).
12. R.S. Hayano *et al.*, Phys. Rev. Lett. **73**, 1485 (1994); *errata*, Phys. Rev. Lett. **73**, 3181 (1994).
13. F.E. Maas *et al.*, Phys. Rev. A **52**, 4266 (1995).
14. H.A. Torii *et al.*, Phys. Rev. A **53**, R1931 (1996).
15. R.S. Hayano *et al.*, Phys. Rev. A **55**, R1 (1997).
16. T. Yamazaki *et al.*, Phys. Rev. A **55**, R3295 (1997).

17. G.T. Condo, Phys. Lett. **9**, 65 (1964).
18. V.I. Korobov, I. Shimamura, Phys. Rev. A **56**, 4587 (1997).
19. T. Yamazaki, K. Ohtsuki, Phys. Rev. A **45**, 7782 (1992).
20. I. Shimamura, Phys. Rev. A **46**, 3776 (1992).
21. R. Pohl *et al.*, Phys. Rev. A **58**, 4406 (1998).
22. T. Yamazaki *et al.*, Chem. Phys. Lett. **265**, 137 (1997).
23. B. Ketzer *et al.*, Phys. Rev. Lett. **78**, 1671 (1997).
24. B. Ketzer *et al.*, J. Chem. Phys. **109**, 424 (1998).
25. H.A. Torii *et al.*, Nucl. Instrum. Meth. Phys. Res. A **396**, 257 (1997).
26. F. Pobell, *Matter and methods at low temperatures* (Springer, Berlin, 1992).
27. M. Hori *et al.*, *errata*, Phys. Rev. A **58**, 1612 (1998).
28. F.J. Hartmann *et al.*, Phys. Rev. A **58**, 3604 (1998).
29. J.B. Hasted, *Physics of atomic collisions*, 2nd edn. (Butterworth & Co., London, 1972).
30. P. Valiron, S. Sauge, J. Carbonell, Results presented at the *Antiprotonic Helium Atomcule Workshop*, Tokyo, Japan, November 26, 1998.
31. R.N. Porter, M. Karplus, J. Chem. Phys. **40**, 1105 (1964).